Astronomy & Astrophysics

X-ray absorption lines suggest matter infalling onto the central black-hole of Mrk 509

M. Dadina[1], M. Cappi[1], G. Malaguti[1], G. Ponti[1,2,3], and A. De Rosa[4]

[1] IASF/INAF Sezione di Bologna, via Gobetti 101, 40129 Bologna, Italy
   e-mail: dadina@bo.iasf.cnr.it
[2] Dipartimento di Astronomia dell'Universitá degli Studi di Bologna, via Ranzani 1, 40127 Bologna, Italy
[3] Institute of Astronomy, Madingley Road, Cambridge CB3 0HA, UK
[4] IASF/INAF, via Fosso del Cavaliere 100, 00133 Roma, Italy

ABSTRACT

Evidence for both red- and blue-shifted absorption lines due to ionized Fe in the X-ray spectrum of the Seyfert 1 galaxy Mrk 509 is reported. These features appear to be transient on time-scales as short as ~20 ks, and have been observed with two different satellites, *BeppoSAX* and *XMM-Newton*. The red- and blue-shifted lines are found at $E \sim 5.5$ keV and ~8.1–8.3 keV (rest-frame), respectively. The first is seen in one out of six *BeppoSAX* observations, the latter is seen by both satellites. Under the assumption that the absorption is due to either H- or He-like Iron, the implied velocities for the absorbing matter are $v \sim 0.15-0.2$ c, in both outward and inward directions. An alternative explanation in terms of gravitational red-shift for the ~5.5 keV line cannot be ruled out with the current data. We argue, however, that the temporal patterns and sporadic nature of the lines are more easily reconciled with models that predict important radial motions close to the central black hole, such as the "aborted jet" model, the "thundercloud" model, or magneto-hydrodynamical models of jets and accretion-disks.

Key words. galaxies: Seyfert – X-rays: individuals: Mrk 509 – black hole physics

1. Introduction

Most popular models adopted to explain the high luminosity of AGNs are based on the release of gravitational energy of infalling matter accreting onto a supermassive black hole (SMBH). Nonetheless there are few direct measurements of matter infall/accretion in AGNs. The most impressive one is probably the detection of a relativistically broadened FeKα line in the X-ray spectrum of the Seyfert 1 galaxy MCG-6-30-15 (Tanaka et al. 1995). Detailed studies of the FeK$_\alpha$ double-horn profile have the potential to trace the matter path in the vicinity of the SMBH. However, recent results obtained with XMM-Newton and Chandra observatories show that data are more complex to interpret than expected (Reeves et al. 2001; Bianchi et al. 2004; Dovciak et al. 2004). Probably the most convincing evidence of matter accreting onto a SMBH, to date is presented by Ponti et al. (2004) on MCG-6-30-15 and by Iwasawa et al. (2004) on NGC 3516. Using two different model-independent and timing tools, these authors showed the existence of a highly variable component at the energies of the putative relativistically broadened and red-shifted wing of the FeKα line.

On the contrary, there is much evidence of matter outflows in AGNs. The most spectacular displays of such matter ejecta are the jets observed in radio-loud AGNs. Recently, absorption and emission line-like features due to outflowing matter have been also detected in the X-ray spectra of some quasars (Pounds et al. 2003a,b; Dadina & Cappi 2004) and Seyfert galaxies (Kaspi et al. 2000; Kaastra et al. 2000; Turner et al. 2004; Reeves et al. 2004).

Nandra et al. (1999) discussed the possible presence of a red-shifted Fe absorption feature in the X-ray spectrum of the Seyfert 1 galaxy NGC 3516. The ASCA data showed a sharp and narrow count drop at $E \sim 5.9$ keV. The line being red-shifted, the authors speculated that the matter was infalling and/or suffering gravitational red-shift close to the central black hole. Recently, further evidence of red-shifted absorption lines in the X-ray spectra of luminous QSOs has been proposed by Yaqoob & Serlemitsos (2005) and Matt et al. (2005).

Mrk 509 ($z = 0.034$, Fisher et al. 1995) has been observed in X-rays several times with a 2–10 keV flux varying between $\sim 2-5 \times 10^{-11}$ erg cm^{-2} s^{-1}. Its X-ray continuum is quite "typical" (photon index $\Gamma \sim 1.6$–1.9, Turner & Pounds et al. 1989; Nandra & Pounds 1994) for a Seyfert 1 galaxy. At energies below ~2 keV the spectrum is dominated by a soft excess that has been modeled by a warm absorber (Reynolds 1997; George et al. 1998), and/or an extra emission component due to ionized reflection or to the big blue bump hard tail (Perola et al. 2000; De Rosa et al. 2004). *BeppoSAX* observations indicated the presence of a reflection component, and of a high energy cut-off at $E \sim 70$ keV (Perola et al. 2000).

Table 1. Observation Log. Column I: name of the observatory; Col. II: name used in the main text to indicate the observation; Col. III: date of the observation; Col. IV: overall duration of the observation; Col. V: *BeppoSAX* MECS or *XMM-Newton* EPIC pn net exposure; Col. VI: 2–10 keV flux.

Satellite	Name	Date	Duration (ks)	Exposure (ks)	$F_{2-10\,keV}$ $(10^{-11}\ \mathrm{erg\ s^{-1}\ cm^{-2}})$
I	II	III	IV	V	VI
BeppoSAX		May 18, 1998	110	52	5.0
BeppoSAX		October 11, 1998	79	36	6.2
XMM-Newton	XMM1	October 25, 2000	31	21	2.6
BeppoSAX		November 3, 2000	87	41	2.9
BeppoSAX		November 8, 2000	85	38	2.5
BeppoSAX		November 18, 2000	93	40	2.5
BeppoSAX	SAX6	November 24, 2000	91	33	2.6
XMM-Newton		April 20, 2001	44	23	4.0

A weak FeK$_\alpha$ emission line was first observed with Ginga at $E = 6.6 \pm 0.3$ keV (Nandra & Pounds 1994), and then confirmed by ASCA (Nandra et al. 1997). This feature was, nonetheless, detected only in 5 out of the 11 ASCA observations (Weaver et al. 2001); in one case, the line was detected at $E \sim 7$ keV.

Broad band ($\sim$0.1–100 keV) analysis of the six *BeppoSAX* observations of Mrk 509 was performed by De Rosa et al. (2004) by merging the two 1998 and the four 2000 observations in two average spectra. These authors compared two alternative models: a cold Compton reflection and a reflection from an ionized disk. For both sets of observations, the authors reported the detection of a narrow and weak FeKα emission line at $\sim$6.4 keV, with equivalent width (*EW*) $\sim$60 and 100 eV, for the 1998 and 2000 observations respectively. The intensity of the line, as well as its constancy and narrowness lead the authors to argue that this component arises from distant, cold and optically thick matter (De Rosa et al. 2004; Yaqoob et al. 2003), probably associated with the optical broad line regions.

XMM-Newton observed Mrk 509 twice. During the first observation (Pounds et al. 2001; Page et al. 2003), a very weak (*EW* $\sim$ 50 eV) and narrow FeKα line was detected at 6.4 keV. Signatures of a possible second line at $E \sim 6.7$–6.9 keV were also observed. To account for this ionized line and to partially explain the soft-excess below 1.5 keV, the authors used a model based on the enhanced reflection due to ionized matter.

2. Data reduction and analysis

We analyzed all the *BeppoSAX* and *XMM-Newton* observations of Mrk 509 (Table 1) although in the next sections our attention is mainly focused on the *BeppoSAX* observation performed on November 24, 2000 (hereafter SAX6) and on the *XMM-Newton* pointing of October 25, 2000 (hereafter XMM1).

Source counts were extracted from circular regions with radius equal to 8′ and 4′ for *BeppoSAX* LECS and MECS, respectively. The LECS, MECS and PDS spectra were rebinned so as to sample the energy resolution of the instruments using grouping files produced by the ASI Science Data Center. To subtract the background, we used standard PHA files accumulated from observations of empty sky regions and produced
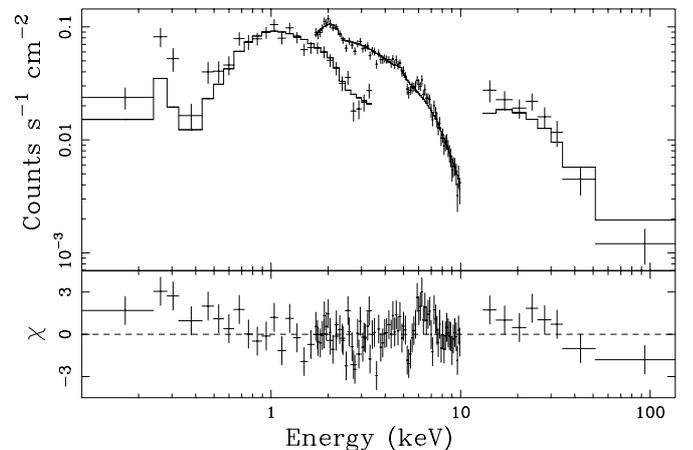

Fig. 1. *Upper panel*: broad-band spectrum of Mrk 509 during the SAX6 observation. *Lower panel*: data-to-model residuals (expressed in terms of standard deviations) assuming a simple power-law model with Galactic absorption.

by the *BeppoSAX* team. We also checked that the results obtained using local backgrounds were consistent with the ones presented here. The LECS and MECS data were used only in the 0.1–3.5 keV and 1.7–10 keV energy ranges respectively, i.e. where the instruments are best calibrated. The most recent calibration files were used for the spectral analysis.

XMM-Newton observed Mrk 509 with the EPIC CCDs operating in small window mode. The extraction regions were circles of 35″ for both source and background. The latest version of SAS was used to reduce the data and latest available calibration files were used in data analysis. Data were rebinned so as to have a minimum of 35 counts per bin.

2.1. SAX6 observation: whole exposure

Figure 1 shows the SAX6 broad band ($\sim$0.1–100 keV) spectrum (upper panel) and residuals (lower panel) when data are fitted with a power-law with Galactic absorption ($N_{\mathrm{H,gal}} \sim 4 \times 10^{20}$ cm^{-2}, Dickey & Lockman 1990). As clearly visible there are some major spectral features, namely a soft X-ray excess below $\sim$1 keV, and some narrow emission and absorption features between $\sim$5–7 keV.

Table 2. Broad band fits of SAX6. Column I: model number; Col. II: photon index; Col. III: relative normalization between the direct and reflected components; Col. IV: energy centroid of the emission line; Col. V: *EW* of the emission line; Col. VI: energy centroid of the absorption line; Col. VII: *EW* of the absorption line; Col. VIII: χ^2 and number of degrees of freedom. Errors are 90% confidence for one interesting parameter.

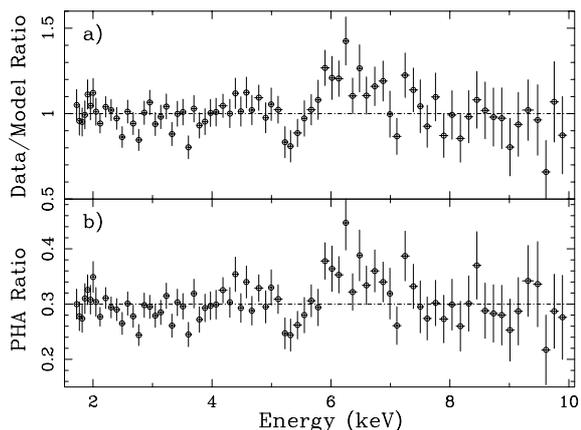| Model	Γ	R	E_{em} keV	EW_{em} eV	E_{ab} keV	EW_{ab} eV	χ^2/d.o.f.
I	II	III	IV	V	VI	VII	VIII
1	$1.61^{+0.11}_{-0.05}$	$0.86^{+0.51}_{-0.60}$	$6.41^{+0.17}_{-0.14}$	143^{+60}_{-61}			110.9/119
2	$1.58^{+0.12}_{-0.05}$	$0.99^{+0.52}_{-0.58}$	$6.37^{+0.18}_{-0.20}$	128^{+111}_{-53}	$5.60^{+0.14}_{-0.12}$	93^{+51}_{-46}	98.5/117

Fig. 2. Panel **a**): data-to-model ratios for SAX6 when the data are fitted with a simple power law model. Panel **b**): PHA ratios between Mrk 509 and 3C 273 *BeppoSAX*.
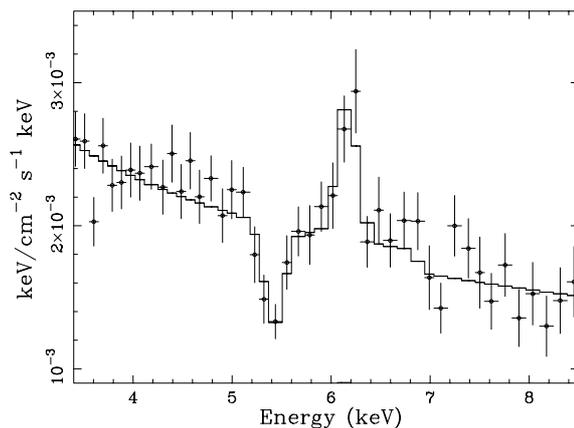

Fig. 3. Unfolded 3–10 keV spectrum measured in SAX6. The continuous line indicates model number 2 in Table 2. In producing the plot, the line widths were fixed to $\sigma = 0.1$ keV for clarity.

Figure 2 (panel a) shows in greater detail the 3–10 keV data-to-model ratios for a simple power law model fit. These clearly indicate an emission feature close to the energies typical of the FeKα line and the possible presence of an absorption feature at $E \sim 5.3$ keV. To exclude that this count drop could be due to a calibration artifact of the response matrices and to adopt a model-independent representation of the data, we calculated the PHA ratios between Mrk 509 and the reference spectrum of 3C 273 acquired on January 9, 2000. 3C 273 was chosen since it ensures very good statistics and has an almost featureless spectrum with a flat photon index similar to the one of Mrk 509 during SAX6. We have checked that the FeKα line known to be present in the *BeppoSAX* spectrum of 3C 273 (Grandi & Palumbo 2004, and references therein) is much too weak (less than ~5% above the continuum) to have a significant impact on our conclusions on the absorption feature measured between 5–6 keV. The PHA ratios (Fig. 2, panel b) are indeed very similar to what is shown in panel a) of Fig. 2, thus excluding response matrix problems and/or an erroneous modeling of the data.

To fit the broad band spectrum, we followed De Rosa et al. (2004) who obtained better statistics by means of a simultaneous fit to the four 2000 pointings of Mrk 509. The first baseline model we tried consists of a flat primary power law ($\Gamma \sim 1.6$), plus a reflection component due to cold matter (namely the PEXRAV model in XSPEC, Magdziarz & Zdziarski 1995), and a superimposed FeKα emission line (Table 2, model 1). At low energies (below ~1.5 keV) the spectrum is dominated by the

contribution of extra components. De Rosa et al. (2004) modeled this excess by adding a couple of black-body components. To avoid the parameters of the fit diverging, we fixed some of them to the best fit values found by De Rosa et al. (2004): the temperatures of the black bodies were set to be 71 and 240 eV, the high energy cut-off was fixed to 83 keV, the inclination angle was fixed to 30° and abundances were fixed to solar values.

The fit improves significantly when a Gaussian absorption line is added to the model ($\Delta\chi^2 = 12.4$ for two more parameters, see model 2 in Table 2), yielding best fit parameters for the line: $E_{ab} = 5.60 \pm 0.14$ keV, and $EW_{ab} = 93 \pm 50$ eV. Best-fit unfolded spectrum and confidence contours for the absorption line parameters are shown in Figs. 3 and 4, respectively.

We also tried a complex photoionized plasma model (namely the SIABS model in XSPEC, Kinkhabwala et al. 2003) to fit the line. Once the ionization state was fixed to FeXXVI, we obtained that the receding velocity of the putative absorbing matter is $v \sim 0.2$ c with a dispersion $\Delta v \sim 3500$ km s^{-1}, while an Iron absorbing column density of $N_{Fe} \sim 1.3 \times 10^{18}$ cm^{-2}. However, these parameters are only poorly constrained by the quality of the present data.

Following De Rosa et al. (2004) we tested also a ionized reflection model (Ross & Fabian 1993). As expected, the available statistics prevents us from firmly constraining all the parameters of the model. In this case, the improvement of the fit corresponds to a $\Delta\chi^2 = 12.1$. The best fit value of the ionization parameter is $\log\xi \sim 3.5$ ($\xi = 4\pi F_x/n_H$, where F_x is the 0.01–100 keV flux illuminating a slab of gas with solar
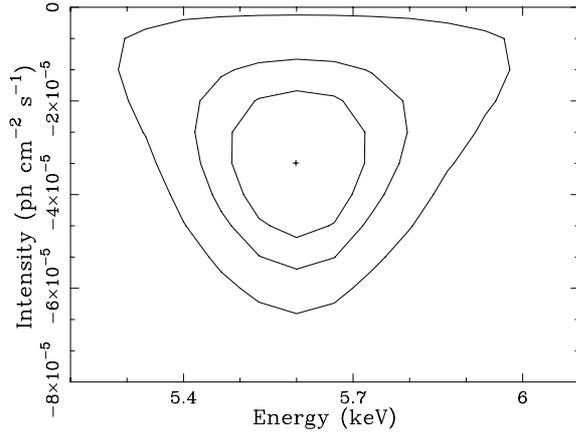
Fig. 4. 99, 90 and 68% confidence contours of the absorption line parameters detected in SAX6 (rest frame energy vs. intensity). The reference X-ray continuum used to calculate these contours is the number 2 in Table 2.
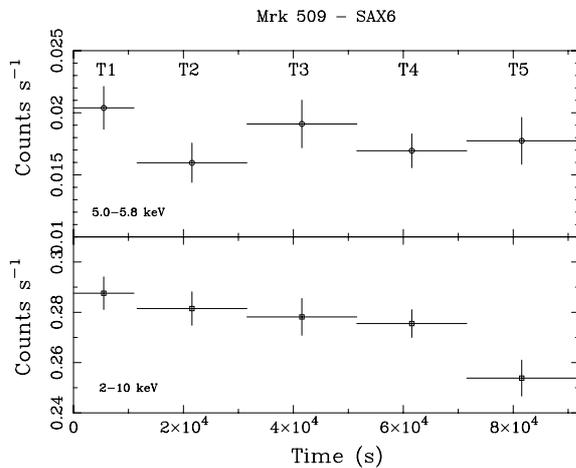

Fig. 5. SAX6 light curves in the 5–5.8 keV range (*upper panel*) and in the 2–10 keV range (*lower panel*).

abundance and constant hydrogen number density $n_H = 10^{15}$ cm^{-3}. The incident flux is assumed to be a power law with a sharp high energy cut-off at $E \sim 100$ keV).

We searched for absorption lines between 5 and 6 keV also in the other *BeppoSAX* and *XMM-Newton* observations but obtained only upper-limits ranging between 10 and 50 eV (at 90% confidence).

2.2. SAX6 observation: time-resolved analysis

The occurrence of such an absorption feature in only one out of six *BeppoSAX* observations of Mrk 509 suggests a sporadic nature. This led us to analyze the SAX6 observation so as to further investigate the feature variability. We found a best trade-off between time resolution and collected photons (available statistics) in dividing the observation in five intervals represented by the time bins of the light curves shown in Fig. 5, where the light curves in the 5–5.8 keV band (upper panel) and in the 2–10 keV band (lower panel) are presented.

To exclude systematic effects, we performed the PHA ratios with 3C273 data also in these time intervals (Fig. 6). During
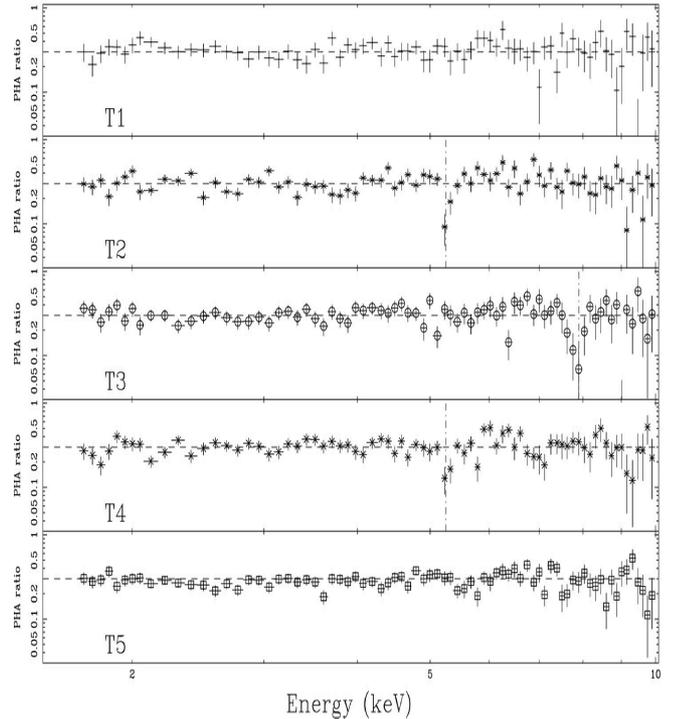

Fig. 6. Mrk 509/3C273 PHA ratios obtained dividing the SAX6 observation in 5 intervals (see text for details).

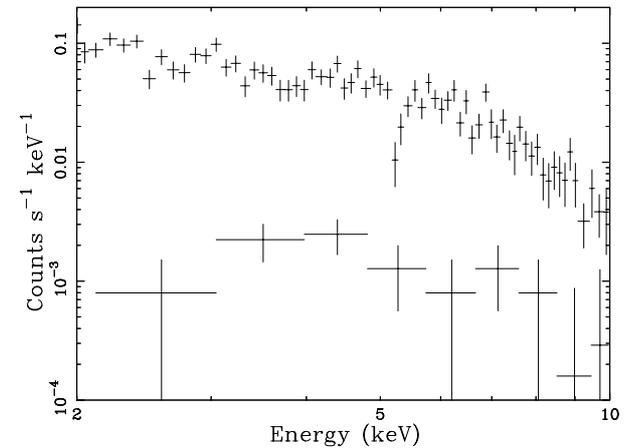**Fig. 7.** Source and local background (2–10 keV) spectra during T2 show how, at the energies of the absorption line, the background contributes to ~5% of the source counts. Similar results are obtained for the T3 and T4 periods.

periods T2, T3 and T4, three different "absorption features" are clearly visible at $E \sim 5.3$ keV (T2 and T4) and 7.9 keV (T3) (observer frame). The count drops account for deviations as large as ~60% and 40% in T2 and T4, respectively.

A check of the relative importance and shape of the background during these short intervals (see Fig. 7 for the T2 interval) confirmed that no anomalous features were present in the local background during T2, T3 and T4 periods.

To model these spectral features we restricted the spectral analysis only to the ~2–10 keV MECS data. The data were fitted with a simple power-law model. We find that the addition of absorption features increases significantly the quality of the

Table 3. Time-resolved analysis of SAX6. Column I: time interval; Col. II: energy centroid of the absorption line; Col. III: line intensity; Col. IV: line EW; Col. V: χ^2 variation after inclusion of an absorption Gaussian line to a simple power law model; Col. VI: F-test significance of the absorption line. Errors are 90% confidence for one interesting parameter.

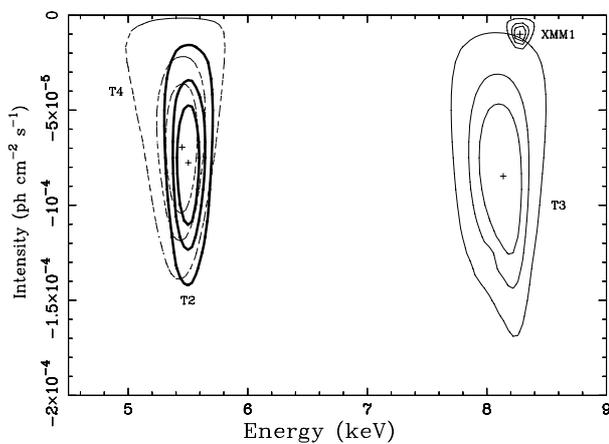| SAX6 period	E	Line intensity	EW_{ab}	$\Delta\chi^2$
	(keV)	(10^{-5} ph s^{-1} cm^{-2})	eV	
I	II	III	IV	V
T2	$5.50^{+0.12}_{-0.12}$	$-7.82^{+3.25}_{-3.49}$	195^{+81}_{-85}	16.8
T3	$8.14^{+0.15}_{-0.13}$	$-8.48^{+4.14}_{-4.49}$	383^{+96}_{-203}	16.4
T4	$5.45^{+0.15}_{-0.15}$	$-6.97^{+3.65}_{-3.66}$	173^{+90}_{-90}	9.6

Fig. 8. Confidence contours for parameters of interest of the absorption features measured during periods T2 (thick solid line), T3 (solid line) and T4 (dashed line) of SAX6 and XMM1. The line width was fixed to $\sigma = 0$ eV. Rest-frame line energies are reported.

Fig. 9. SAX6 time resolved analysis. Panel **a)**: 5.5 keV absorption feature EW_{ab} vs. time intervals. The EW_{ab} obtained during T1, T3 and T5 have been obtained fixing the absorption line energy at 5.5 keV (rest-frame). The continuum is fitted by a simple power-law model. Panel **b)**: same as panel **a)** with line energy fixed at 8.1 keV (rest-frame). Error bars and upper limits are at 90% confidence level.

2.3. XMM-Newton observation of Oct. 25, 2000 (XMM1)

This observation was previously analyzed by Page et al. (2003). These authors commented on the presence of residuals at $E \sim 8$ keV in their best-fit model, but did not attempt to model them. Fitting the 2–10 keV data with a simple power-law, the addition of a narrow absorption line at $E = 8.27 \pm 0.05$ keV with an $EW_{ab} = 40 \pm 20$ eV leads to a reduction of the $\Delta\chi^2 = 12.5$ (Fig. 8). As for SAX6, the modeling of this absorption feature with an edge leads to a worse fit ($\Delta\chi^2 \sim 10$ for the same number of degrees of freedom).

In this energy range, the background of the EPIC CCDs is strongly affected by a Cu activated emission line. The net effect of an inadequate removal of this background feature could, in principle, cause the presence of an absorption and/or emission feature in the source spectrum.

We tested this possibility by using different background regions. This did not significantly change the results on the absorption line parameters. Moreover, at the energy of the absorption feature, the background contributes ≲5% to the source counts (Fig. 10), thus excluding that the ~8 keV absorption feature is due to background subtraction problems.

2.4. Other BeppoSAX and XMM-Newton observations of Mrk 509

We performed a time-resolved search for absorption features in the other observations of Mrk 509 performed by *BeppoSAX* and *XMM-Newton*, but without success. This confirms that these features are of transient nature and partially explains why these features were not detected before even though the same data were already analyzed. Moreover, the occurrence of these features seems to be independent of the source state. Thus a bias against their detection is expected since they are expected to be washed out in spectra averaged over long exposures.

fit in T2, T3 and T4 (see Table 3). The addition of a narrow or broad FeK$_\alpha$ emission line is not required by the data but we found that the absorption line detections are also robust to the inclusion of either narrow or broad emission lines above and/or below the absorption line energy.

Figure 8 shows the confidence contours plots for the (rest frame) parameters of interest of these absorption lines. The line widths are consistent with the instrumental energy resolution. We also tried to fit the feature at ~8 keV during T3 with an absorption edge but the result was a poorer fit ($\Delta\chi^2 \sim 14$ for the same degrees of freedom) when compared to that obtained with the absorption Gaussian line.

We searched for variability in the absorption lines by fixing their energy at 5.5 and 8.1 keV, and computing the corresponding intensities during T1 to T5 with respect to a simple power law model. The 90% upper limit on EW_{ab} during T5 is not consistent with what was measured in T2 (panel (a) of Fig. 9) and only marginally with T4. On the other hand, the ~8.1 keV feature detected in T3 is well above the 90% upper limits obtained in the other time intervals (panel (b) of Fig. 9).
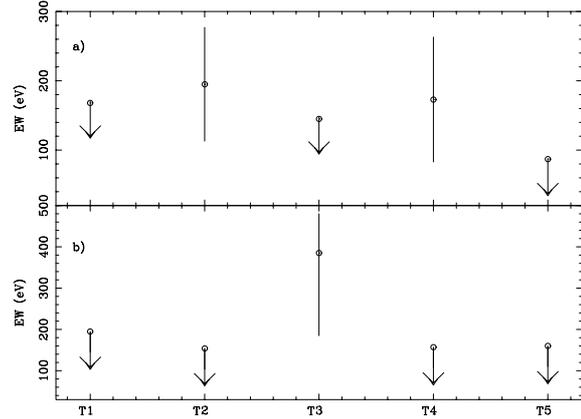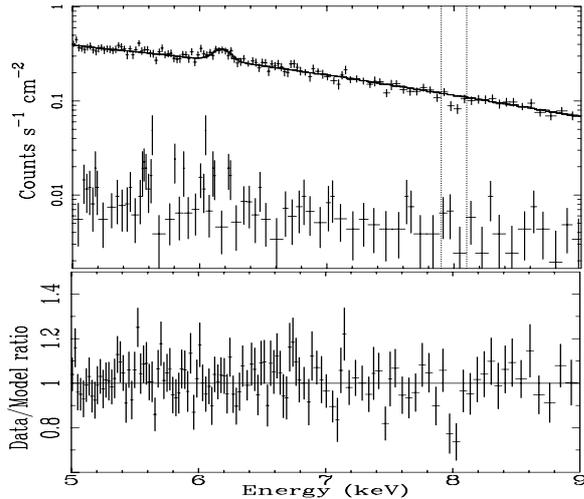
Fig. 10. *Upper panel*: source and background (5–9 keV) spectra during XMM1. Dotted lines highlight the energy range of the detected absorption line. A FeKα narrow emission line has been added to the model. *Lower panel*: data-to-model ratio with respect to a spectral model composed by a power-law plus an narrow emission line.

2.5. On the significance of the absorption lines

A word of caution should be stated here for the statistical significance of the absorption lines detected in SAX6 and XMM1 at ~5.5 and ~8.2 keV, respectively. If the F-test is applied to these observations, the output is that these features are significant to a ~99.9% confidence level. Nonetheless this does not account for the total number of trials performed, as well as for the total number of resolution elements used for the line detection (see, e.g., Protassov et al. 2002; Porquet et al. 2004; Yaqoob & Serlemitsos 2005). If we consider only the 5.5 keV feature and the average spectra, we find that the F-test significance decreases to ~99.2% because of the number of trials involved (the eight *BeppoSAX* and *XMM-Newton* observations). The same arguments could be applied for the time-resolved analysis (a total of 33 time resolved spectra) thus reducing the overall significance in detecting a single absorption line at ~96.7%. Moreover, Protassov et al. (2002) discussed how the F-test like indicators could fail in assessing the real significance of an absorption feature, overestimating it. We cannot, therefore, strongly fix the "true" significance of our results that could be possibly, lower than deduced by the application of the F-test.

It is encouraging, however, that the four lines detected with the time resolved analysis of the data have been found to be consistent with only two energies. Moreover detections of both blue- and red-shifted lines have been claimed by some authors (Pounds et al. 2003a,b; Yaqoob & Serlemitsos 2005; Matt et al. 2005), thus suggesting that the features reported here are not a statistical artifact. Confirmations with instruments with larger collecting area and/or greater energy resolutions, are needed to definitively fix the significance of the spectral and time patterns measured here.

3. Discussion

Evidence for absorption features in the X-ray spectrum of Mrk 509 has been detected at ~5.5 keV (twice in BeppoSAX data) and at ~8.2 keV (in both *BeppoSAX* and *XMM-Newton* non-simultaneous data). Both features appear to be transient on time scales that could be as short as ~20 ks.

As previously proposed for other Seyferts and QSOs, the most natural explanation of such narrow components is in terms of both blue-shifted and red-shifted resonant absorption lines from H-like or He-like Iron (Nandra et al. 1999; Pounds et al. 2003a; Reeves et al. 2003; Longinotti et al. 2003; Yaqoob & Serlemitsos 2005; Matt et al. 2005). This is also consistent with the fact that the best-fit of the spectrum requires an ionized reflection component with $\log \xi \sim 3.5$, thus implying the presence of FeXXV and FeXXVI (De Rosa et al. 2004).

If associated with FeXXVI (6.96 keV rest-frame), the inferred shifts in energy correspond to receding velocities of (0.21 ± 0.02) c (T2 and T4) and to approaching velocities of (0.16 ± 0.02) c (T3) and (0.19 ± 0.02) c (XMM1). If associated mainly with FeXXV (6.7 keV rest-frame), the velocities become ~0.18, 0.20 and 0.23 c, respectively.

Nandra et al. (1999) first discussed the interesting possibility that the red-shifted line seen in NGC 3516 could be the direct signature of matter inflow/infall. Alternatively, Ruszkowski & Fabian (2000) explained how the NGC 3516 feature could be due to a warm plasma surrounding the X-ray source. In their picture, the absorbing matter is located close to the black hole and the resonant absorption line is red-shifted by the gravitational field produced by the SMBH. A similar interpretation has been given by Yaqoob & Serlemitsos (2005) for the red-shifted Iron line observed with the Chandra HETG in the QSO E1821+643. Present results cannot rule out that the line red-shifts measured in T2 and T4 are partially or even totally due to gravitational red-shift. Nonetheless, the data seem to require either a transient or an "un-steady" absorber in order to explain the sporadic presence of the absorption features.

The temporal succession of the absorption events measured in T2-T3-T4 (red-blue-red shifts) seems to indicate a physical relation between the red and blue-shifted components. The present data, in fact, suggest a picture in which we are observing the succession of matter infalls and ejecta that sporadically obscure the X-ray continuum source, i.e. indicating the presence of non-circular motions close to the SMBH. The use of the SIABS model (see Sect. 2.1, Kinkhabwala et al. 2003) to fit the entire SAX6 data gives an Iron column density $N_{\rm Fe} \sim 1.3 \times 10^{18}$ cm^{-2} for the red-shifted lines, which, assuming solar abundances, corresponds to a total column of $N_{\rm H} \sim 6 \times 10^{22}$ cm^{-2}. Considering the $EW_{\rm ab}$ obtained in shorter periods and using the "curves of growth" presented in Kotani et al. (2000), we obtained the absorbing columns: $N_{\rm H} \sim 1.3 \times 10^{23}$ cm^{-2} in T2-T3-T4 and $N_{\rm H} \sim 4 \times 10^{22}$ cm^{-2} in XMM1. Assuming 20 ks (i.e. the duration of T2, T3, and T4) as the characteristic variability timescale, the upper limit to the dimensions of the absorbing regions can be estimated to be $d \sim 6 \times 10^{14}$ cm. This leads to an upper limit on the mass involved of ~0.3–1.2 × 10²⁸ g (~1.5–6 × 10⁻⁵ $M_\odot$), depending on the geometry of the absorber. The related density

lower limit is, thus, $\sim 0.5\text{--}2 \times 10^8$ atoms cm^{-3}. From the measured velocity $v \sim 0.2$ c it is then possible to infer the kinetic energy of the moving matter $E_{kin} \leq \Gamma Mc = 9 \times 10^{47}$ erg, where Γ is the bulk Lorentz factor and M is the absorber mass. The difference between the column densities measured in SAX6 and XMM1 indicates that either the density or the geometry or the ionization state of the intervening matter has varied between the two epochs ($\sim$one month apart).

Our results are in good agreement with what is predicted by the "aborted jet" model for the production of X-rays in radio-quiet AGN (Ghisellini et al. 2004). In this framework, X-rays are produced via the extraction of rotational energy from the BH by repeated expulsions of blobs/clouds of matter with initial speed below the escape velocity. The collisions between blobs determine the transmission of a significant amount of the kinetic energy to the gas contained in the blobs. This generates a hot plasma that Comptonizes to X-rays the seed UV photons from the accretion disk. At the end of the process, about 5–10% of the initial kinetic power is transformed into X-rays that dominate the nuclear emission when the source is in high luminosity states. From our data we can estimate the jet power ignition to be $\sim E_{kin}/t_{obs}$ ($\leq 10^{44}$ erg s^{-1}), where t_{obs} is the total length of the SAX6 observation. Thus, during SAX6 and XMM1, the "aborted jet" contributes less than 5–10% to the total X-ray luminosity observed. This value is in agreement with theory since it is expected that the jet contribution to the X-ray emission is negligible during the low luminosity states like SAX6 and XMM1. In fact, these are predicted to be dominated by the disk-corona X-ray emission.

Finally, our results are qualitatively in agreement also with more traditional models. Magneto-hydrodynamic (MHD) simulations of the matter inflow onto a black hole via an accretion disk (De Villiers et al. 2003) predict that the accretion flow of the disk is almost stable, but, close to the SMBH, local instabilities may lead to the formation of infalling blobs/winds. Coupled with the accretion flow, these simulations also predict outflows of warm/hot matter that supply the corona with both gas and magnetic energy, and lead to the formation of high velocity ejecta. Similarly, what is observed in Mrk 509 may be interpreted in the view of the "Thundercloud model" (Merloni & Fabian 2001) that predicts turbulent motion of gas in a "patchy corona" over the accretion disk. In this framework, corona/disk instabilities could produce episodes of matter ejecta and infalls.

4. Conclusions

Understanding gas inflows/outflows in AGNs gives insight into accretion/expulsion processes, two of the most fundamental questions regarding black hole systems. To date, data from several Seyfert galaxies and QSOs show signatures of narrow, blue-shifted absorption lines explained as due to Iron resonant absorption in outflowing gas. In this work, we report evidence of both red-shifted and blue-shifted transient absorption lines in the X-ray spectrum of the Seyfert galaxy Mrk 509. If confirmed, the red-shifted lines would be particularly interesting because they could be one of the best direct evidence of matter free-falling onto a SMBH. The data presented here are in good agreement with most theoretical models that imply important radial motions close to the SMBH (such as, for example, the "aborted jet" model). Other scenarios that explain the line redshifts in terms of gravitational red-shift cannot be ruled out but seem to require a higher degree of complexity to account for the pattern and sporadic nature of the absorption lines. A detailed analysis of the line profile is needed in order to test these hypotheses. If confirmed, these results may offer new potential to study the kinematics and dynamics of the gas close to the SMBH via detailed absorption line X-ray spectroscopy. If the inflow is due to a wind rather than blobs, one would expect the features to exhibit a typical inverted P-Cygni profile (Edwards et al. 1994). On the other hand, a blob scenario, as favored here, would provide test-particles suitable to verify predictions of General Relativity in strong gravitational fields.

References

Bianchi, S., Matt, G., Balestra, I., Guainazzi, M., & Perola, G. C. 2004, A&A, 422, 65

Dadina, M., & Cappi, M. 2004, A&A, 413, 921

De Rosa, A., Piro, L., Matt, G., & Perola, G. C. 2004, A&A, 413, 895

De Villiers, J., Hawley, J. F., & Krolik, J. H. 2003, ApJ, 599, 1238

Dickey, J. M., & Lockman, F. J. 1990, ARA&A, 28, 215

Dovčiak, M., Bianchi, S., Guainazzi, M., Karas, V., & Matt, G. 2004, MNRAS, 350, 745

Edwards, S., Hartigan, P., Ghandour, L., & Andrulis, C. 1994, AJ, 108, 1056

Fisher, K. B., Huchra, J. P., Strauss, M. A., et al. 1995, ApJS, 100, 69

Iwasawa, K., Miniutti, G., & Fabian, A. C. 2004, MNRAS, 521

George, I. M., Turner, T. J., Netzer, H., et al. 1998, ApJS, 114, 73

Ghisellini, G., Haardt, F., & Matt, G. 2004, A&A, 413, 535

Grandi, P., & Palumbo G. G. C, 2004, Science, 306, 998

Kaastra, J. S., Mewe, R., Liedahl, D. A., Komossa, S., & Brinkman, A. C. 2000, A&A, 354, L83

Kaspi, S., Smith, P. S., Netzer, H., et al. 2000, ApJ, 533, 631

Kinkhabwala, A., Behar, E., Sako, M., et al. 2003, in press [arXiv:astro-ph/0304332]

Kotani, T., Ebisawa, K., Dotani, T., et al. 2000, ApJ, 539, 413

Longinotti, A. L., Cappi, M., Nandra, K., Dadina, M., & Pellegrini, S. 2003, A&A, 410, 471

Magdziarz, P., & Zdziarski, A. A. 1995, MNRAS, 273, 837

Matt, G., Porquet, D., Bianchi, S., et al. 2005, A&A, 435, 857

Merloni, A., & Fabian, A. C. 2001, MNRAS, 328, 958

Nandra, K., & Pounds, K. A. 1994, MNRAS, 268, 405

Nandra, K., George, I. M., Mushotzky, R. F., Turner, T. J., & Yaqoob, T. 1997, ApJ, 477, 602

Nandra, K., George, I. M., Mushotzky, R. F., Turner, T. J., & Yaqoob, T. 1999, ApJ, 523, L17

Page, M. J., Davis, S. W., & Salvi, N. J. 2003, MNRAS, 343, 1241

Perola, G. C., Matt, G., Fiore, F., et al. 2000, A&A, 358, 117

Ponti, G., Cappi, M., Dadina, M., & Malaguti, G. 2004, A&A, 417, 451

Porquet, D., Reeves, J. N., Uttley, P., & Turner, T. J. 2004, A&A, 427, 101

Pounds, K., Reeves, J., O'Brien, P., et al. 2001, ApJ, 559, 181

Pounds, K. A., King, A. R., Page, K. L., & O'Brien, P. T. 2003a, MNRAS, 346, 1025

Pounds, K. A., Reeves, J. N., King, A. R., et al. 2003b, MNRAS, 345, 705

Protassov, R., van Dyk, D. A., Connors, A., Kashyap, V. L., & Siemiginowska, A. 2002, ApJ, 571, 545

Reeves, J. N., Turner, M. J. L., Pounds, K. A., O'Brien, P. T., & Page, K. 2001, New Century of X-ray Astronomy, ASP Conf. Ser., 251, 120

Reeves, J. N., O'Brien, P. T., & Ward, M. J. 2003, ApJ, 593, L65

Reynolds, C. S. 1997, MNRAS, 286, 513

Ross, R. R., & Fabian, A. C. 1993, MNRAS, 261, 74

Ruszkowski, M., & Fabian, A. C. 2000, MNRAS, 315, 223

Tanaka, Y., Nandra, K., Fabian, A. C., et al. 1995, Nature, 375, 659

Turner, T. J., Kraemer, S. B., & Reeves, J. N. 2004, ApJ, 603, 62

Turner, T. J., & Pounds, K. A. 1989, MNRAS, 240, 833

Weaver, K. A., Gelbord, J., & Yaqoob, T. 2001, ApJ, 550, 261

Yaqoob, T., McKernan, B., Kraemer, S. B., et al. 2003, ApJ, 582, 105

Yaqoob, T., & Serlemitsos, P. 2005, ApJ, 623, 112